Eur. Phys. J. Spec. Top.
https://doi.org/10.1140/epjs/s11734-024-01102-9

THE EUROPEAN PHYSICAL JOURNAL SPECIAL TOPICS

Regular Article

Slepton searches in the trilinear RPV SUSY scenarios at the HL-LHC and HE-LHC

Arghya Choudhury[1,a], Arpita Mondal[1,b], Subhadeep Mondal[2,c], and Subhadeep Sarkar[1,d]

[1] Department of Physics, Indian Institute of Technology Patna, Patna, Bihar 801106, India
[2] Department of Physics, SEAS, Bennett University, Greater Noida, Uttar Pradesh 201310, India

Received 15 September 2023 / Accepted 19 January 2024

Abstract In this work, we have studied a multi-lepton final state arising from sneutrino and left-handed slepton production at the high-luminosity and high-energy LHC in the context of R-parity violating supersymmetry when only the lepton number violating λ_{121} and/or λ_{122} couplings are non-zero. We have taken into account both pair production and associated production of the three generations of left-handed sleptons and sneutrinos, which are assumed to be mass degenerate. The lightest supersymmetric particle is assumed to be bino and it decays via the R-parity violating couplings into light leptons and neutrinos. Our final state has a large lepton multiplicity, $N_l \geq 4$ ($l = e,\ \mu$). We perform both cut-based and machine learning-based analyses for comparison. We present our results in the bino-slepton/sneutrino mass plane in terms of exclusion and discovery reach at the LHC. Following our analysis, the slepton mass can be discovered up to $\sim$ 1.54 TeV and excluded up to $\sim$ 1.87 TeV at the high-luminosity LHC, while these ranges go up to $\sim$ 2.46 and $\sim$ 3.06 TeV, respectively, at the high-energy LHC.

1 Introduction

The LHC collaborations have meticulously looked for the signal beyond Standard Model (BSM) physics using Run-I and Run-II data and will do the same with ongoing Run-III operations. Supersymmetry [1–4] is still the most popular and promising BSM scenario that solves various shortcomings of the standard model (SM)—e.g., the gauge hierarchy problem [5, 6], observed dark matter (DM) relic density of the universe [7], muon (g-2) anomaly [8], etc. As there are still no hints of new physics signal from the LHC Run-I and Run-II data, the lower bound on strongly interacting colored sparticle masses have reached up to $\mathcal{O}$(2–2.5) TeV [9, 10]. On the other hand, the bounds on the electroweak (EW) sector SUSY particles are much weaker [9, 10]. The R-parity conserving (RPC) minimal supersymmetric standard model (MSSM) [1–4, 11] provides a stable weakly interacting massive particle (WIMP) which can be a natural DM candidate [12–15] and the most popular choice is the lightest neutralino ($\widetilde{\chi}_1^0$) in the form of lightest SUSY particle (LSP). In the RPC scenarios with light EW sectors, there are a large number of phenomenological analyses which have addressed the implication of LHC results along with muon (g-2) anomaly and observed DM relic density data [16–26].

The RPC MSSM is more extensively studied in literature due to the DM candidate in the form of the LSP, and for that we need to incorporate the R-parity conservation by hand. If R-parity violating (RPV) terms are allowed, the superpotential looks like [27–30]

$$W_{\not{R}_p} = \mu_i \hat{H}_u.\hat{L}_i + \frac{1}{2}\lambda_{ijk}\hat{L}_i.\hat{L}_j\hat{e}^c_k + \frac{1}{2}\lambda'_{ijk}\hat{L}_i.\hat{Q}_j\hat{d}^c_k + \frac{1}{2}\lambda''_{ijk}\hat{u}^c_i\hat{d}^c_j\hat{d}^c_k \tag{1}$$

where the first three terms are the lepton number violating terms and the last term violates the baryon number. Here, $\hat{H}_u$ is the up-type Higgs supermultiplet and $\hat{L}$ ($\hat{e}$) refers to the left-handed lepton doublet (right-handed

[a] e-mail: arghya@iitp.ac.in (correspondingauthor)
[b] e-mail: arpita_1921ph15@iitp.ac.in
[c] e-mail: subhadeep.mondal@bennett.edu.in
[d] e-mail: subhadeep_1921ph21@iitp.ac.in

Published online: 09 February 2024

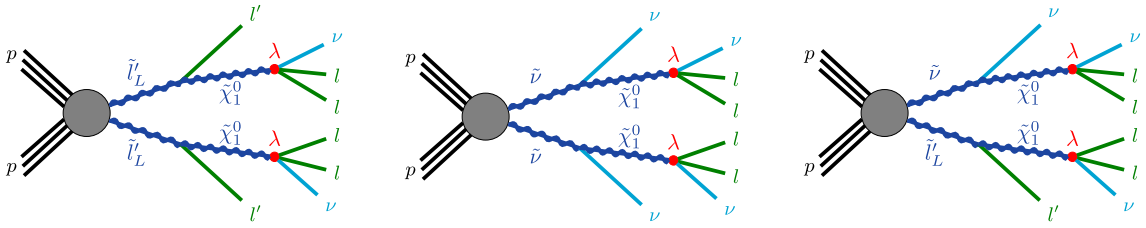

Fig. 1 Diagrams for decays of $\tilde{l}'_L$, $\tilde{\nu}$ to $\tilde{\chi}^0_1$ and $\tilde{\chi}^0_1$ decays to leptons via λ coupling. Here $l' = e$, μ, τ and $l = e$, μ

singlet) supermultiplet. Similarly, $\hat{Q}$ ($\hat{u}$) corresponds to the up-type left (right)-handed doublet (singlet) quark supermultiplet. $\hat{d}$ represents the right-handed down-type quark supermultiplet. In this work, we only consider the non-zero λ couplings[1] which have distinctive collider signatures compared to RPC scenarios. In the RPC scenario, the stable LSP leads to a large amount of missing energy $\not{E}_T$ in the final states while the LSP decays to multilepton final states for $\lambda_{ijk} \neq 0$ scenarios. Depending on the choices of LSP and non-zero RPV couplings, one obtains various novel final states [34–39]. For different choices of λ_{ijk} couplings, the LHC collaborations have already derived limits on chargino and slepton masses [40] using LHC Run-II data and it will be interesting to study the sensitivity of the EW sparticle searches at the 14 TeV high-luminosity LHC (HL-LHC) and the proposed high-energy (27 TeV) upgrade of the LHC (HE-LHC). It may be noted that the SUSY parameter space containing one or more lighter EW sparticles like charginos, sneutrinos, smuons or neutralinos are very much consistent with the recent measurement of muon magnetic moment at Fermilab [8, 41, 42]. The additional contributions from SUSY mainly come from the chargino–sneutrino loop and smuon–neutralino loop and there could be even some additional contribution in the RPV scenarios depending on the couplings. A few phenomenological analyses with RPC and RPV scenarios in the context of muon (g-2) anomaly may be seen in Refs. [17, 23, 33, 43–54].

In a recent work [55], the searching prospect of gaugino sector at the HL-LHC and HE-LHC with $\mathcal{L} = 3000$ fb^{-1} is presented using the direct $\widetilde{\chi}^{\pm}_1\widetilde{\chi}^{\mp}_1$ and $\widetilde{\chi}^{\pm}_1\widetilde{\chi}^0_2$ production for scenarios with non-zero λ_{ijk} couplings.[2] In this work, we extend a similar analysis using the direct production of mass degenerate L-type sleptons of all three generations. First, we look for the results using traditional cut-and-count-based analysis and then look for the improvement of sensitivity using a machine learning (ML) algorithm. For the ML analysis, we will adopt the boosted decision tree (BDT) [57, 58] algorithm.

In Sect. 2, we discuss the model framework along with the possibility of different final states arising from distinct choice of RPV couplings. In Sect. 3, we first present the projected exclusion limits in the slepton–LSP mass plane using a traditional cut-and-count analysis followed by an ML-based algorithm at the HL-LHC. We extend this multilepton analysis for the HE-LHC also. We conclude our results in Sect. 4.

2 Model definition

The pair production cross sections for L-type charged slepton is roughly ~ 3 times larger than the R-type charged slepton pair production [59–64]. In the context of RPC slepton searches, the most popular simplified models consist of both L and R-type charged slepton of the first two generations. On the other hand, the sneutrino pair productions or charged slepton–sneutrino productions contribute to the multilepton final states in the RPV SUSY scenarios with nonzero λ_{ijk} couplings. In this work, we consider a simplified model where all three generations L-type charged sleptons and sneutrinos are mass degenerate (R-type sleptons are assumed to be lying beyond the reach of the LHC) and the sleptons are produced via $pp \to \tilde{l}'_L\tilde{l}'_L$, $\tilde{\nu}\tilde{\nu}$ and $\tilde{l}'_L\tilde{\nu}$ channels, where $l' \equiv e$, μ, τ. The corresponding Feynman diagrams for these productions are shown in Fig. 1.

Here, the sleptons decay to lepton and bino-type LSP ($\widetilde{\chi}^0_1$) and via the λ_{ijk} couplings the LSP decays into $l'^{\pm}_k l'^{\mp}_{i/j}\nu_{j/i}$, where $l' = e$, μ, τ. Thus, one obtains maximally enriched leptonic final states in scenarios with non-zero λ_{121} and/or λ_{122} couplings, where the LSP pair in the final state always gives rise to $4l$ ($l = e$, μ) + $\not{E}_T$ topology.[3] Depending upon the production modes ($\tilde{l}'_L\tilde{\nu}_L$ and $\tilde{l}'_L\tilde{l}'_L$), one or two more leptons may arise in the final state. In this work, we will focus on non-zero λ_{12k} ($k \in 1, 2$) scenarios and consider the final states consisting of at least four leptons $N_l \geq 4$, where $l \equiv e$, μ. It may be noted that nine non-zero λ_{ijk} couplings lead to different charged lepton configurations and the LSP pair in the final states leads to three more different scenarios where the

[1] These couplings contribute to light neutrino masses and mixings at one loop level [28, 31] and to muon (g-2) [32, 33].
[2] For electroweakino searches in the context of *UDD* couplings at the HL-LHC, please refer to [56].
[3] For example, $\widetilde{\chi}^0_1$ decays to $ee\nu_\mu$ and $e\mu\nu_e$ with 50% branching ratios each for single non-zero values of λ_{121} coupling.

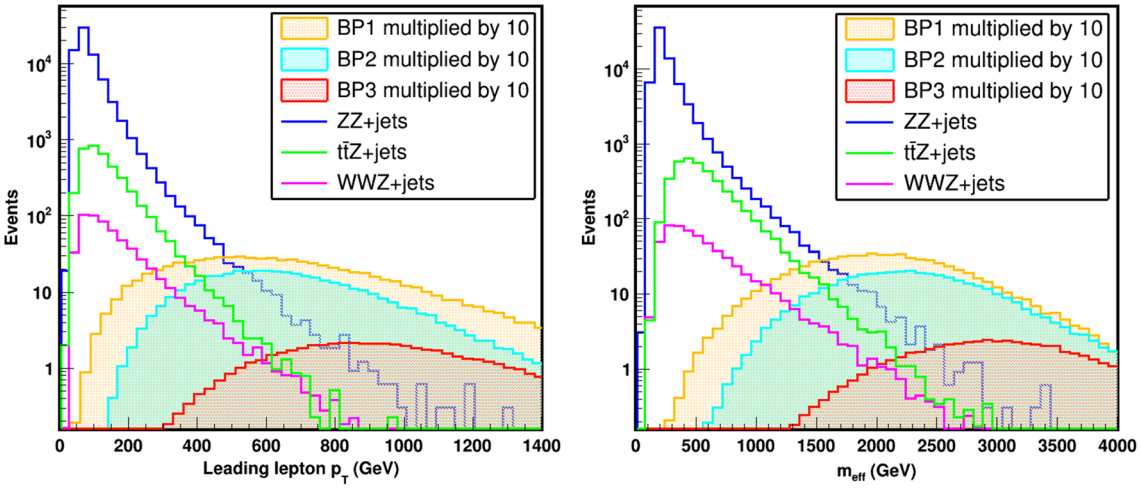

Fig. 2 Distributions of transverse momentum of leading lepton—$p_T^{l_1}$ (left) and effective mass—m_{eff} (right) at the HL-LHC ($\sqrt{s} = 14$ TeV with $\mathcal{L} = 3000\ fb^{-1}$) are shown here. The blue, green, and magenta color solid lines represent the most dominant $ZZ + jets$, $t\bar{t}Z + jets$ and $WWZ + jets$ backgrounds. Yellow, cyan, and red filled regions correspond to the benchmark points—`BP1`, `BP2`, and `BP3`, respectivel,y with a multiplication factor of 10

leptonic ($l = e, \mu$) branching ratios get reduced and the collider limits or sensitivity become weaker .[4] For more details on the LSP decay modes and charged lepton configurations for various scenarios, see Appendix A.

3 Collider analysis

As discussed in the previous section, we consider a simplified model with L-type mass degenerate charged sleptons and sneutrinos (all three generations) and look for the projection reach at the HL-LHC and HE-LHC using a final state with at least four leptons ($N_l \geq 4$). For this final state, dominant SM backgrounds are $ZZ + jets$, $WWZ + jets$ and $t\bar{t}Z + jets$ and we also compute sub-dominant processes like $WZZ + jets$, $ZZZ + jets$, h production via ggF, hjj, $Wh + jets$, $Zh + jets$. All these SM backgrounds and the SUSY signals were generated using `MadGraph5-aMC@NLO` [65] and `Pythia-6.4` [66] at the leading order (LO) parton level, respectively. The cross sections for the SM backgrounds are taken from Table 11 and Table 13 of Ref. [55]. The NLO+NLL level cross sections for SUSY signals were calculated using `Resummino-3.1.1` [59–64]. For fast detector simulation, we have used `DELPHES 3` (version-3.5.0) platform [67]. Jet reconstructions are done using anti-k_t algorithm [68] with jet radius $R = 0.4$, $p_T > 20$ and $|\eta| < 2.8$. Leptons are reconstructed with $p_T > 7$ (5) and $|\eta| < 2.47$ (2.7) cuts from electron (muon) candidates after isolation. The track and calorimeter isolation, $b-$tagging efficiency, generation-level cuts, jet matching, etc., are done in a similar way as prescribed in Sec. 3 of Ref. [55].

3.1 Prospect at the HL-LHC: cut-based vs. ML analysis

In this section, we present the prospect of slepton pair productions at the high-luminosity LHC (HL-LHC) with $N_l \geq 4$ final state at the center of mass energy $\sqrt{s} = 14$ TeV and $\mathcal{L} = 3000$ fb^{-1}. First, we will present the conventional cut-and-count analysis and then we will look for the improvement using a boosted decision tree (BDT)-based machine learning algorithm. In our analysis, we have considered three production channels: (i) $pp \to \tilde{l}'_L \tilde{l}'_L$, (ii) $pp \to \tilde{l}'_L \tilde{\nu}$, and (iii) $pp \to \tilde{\nu}\tilde{\nu}$, where the left-handed sleptons and sneutrinos across all three generations are mass degenerate. Here, $l' = e, \mu, \tau$ and subscript L denotes the left-handed chirality. The individual contribution of the three production channels to the final cross section remains almost similar across all data points (for both the HL-LHC and HE-LHC analysis), where $pp \to \tilde{l}'_L \tilde{\nu}$ process shares the largest contribution ($\sim 65\%$), followed by channel $pp \to \tilde{l}'_L \tilde{l}'_L$ ($\sim 20\%$) and $pp \to \tilde{\nu}\tilde{\nu}$ ($\sim 15\%$). The individual cross sections for each production channel for different benchmark points for the HL-LHC and HE-LHC analysis are shown in Table 8 in Appendix B.

The ATLAS collaboration has already excluded the slepton mass up to 1.2 TeV using RUN-II LHC data [40] for non-zero λ_{12k} ($k \in 1, 2$) couplings. Following the ATLAS analysis [40] and similar to our previous work [55], we optimize the effective mass (m_{eff}) variable for cut-based analysis to maximize the signal significance and define

[4] Before concluding our results, we will also briefly comment on the sensitivity in such scenarios.

Table 1 Production cross sections, selection cuts, and the corresponding yields at the HL-LHC for the three signal benchmark points are presented. The total SM background yields are also shown. The last three rows represent the signal significance ($\sigma^0_{\rm ss}$) without any systematic uncertainty and $\sigma^5_{\rm ss}$ (with Sys. Unc. $\epsilon = 5\%$) for the benchmark points

	$N_l \geq 4$ ($l = e, \mu$) + $p_T^{l_1} > 100$ GeV	Z veto	b veto	Signal region	
				SR-A ($m_{\rm eff} > 900$ GeV)	SR-B ($m_{\rm eff} > 1500$ GeV)
BP1 (1300,250) $\sigma^{14}_{\rm NLO+NLL} = 0.0381\ fb$	74.45	65.28	60.87	59.16	49.10
BP2 (1450,800) $\sigma^{14}_{\rm NLO+NLL} = 0.0196\ fb$	42.20	40.99	38.01	37.80	34.01
BP3 (1800,1750) $\sigma^{14}_{\rm NLO+NLL} = 0.0029\ fb$	5.86	5.56	5.20	5.19	5.10
Total background	22124.17	382.82	221.92	20.19	3.498
Signal significance $\sigma^0_{\rm ss}$ ($\sigma^5_{\rm ss}$, sys. unc. $\epsilon = 5\%$)		BP1		6.64 (6.07)	6.77 (6.36)
		BP2		4.96 (4.64)	5.55 (5.31)
		BP3		1.03 (0.998)	1.74 (1.72)

the signal regions. To demonstrate the results, we consider three signal benchmark points: BP1: $m_{\widetilde{l}_L} = 1300$ GeV, $m_{\widetilde{\chi}^0_1} = 250$ GeV; BP2: $m_{\widetilde{l}_L} = 1450$ GeV, $m_{\widetilde{\chi}^0_1} = 800$ GeV; BP3: $m_{\widetilde{l}_L} = 1800$ GeV, $m_{\widetilde{\chi}^0_1} = 1750$ GeV. The mass difference between sleptons and the LSP is large, intermediate, and small for BP1, BP2, and BP3, respectively. In Fig. 2, we depict the distribution of leading lepton transverse momentum ($p_T^{l_1}$) and effective mass ($m_{\rm eff}$)[5] for the three benchmark points along with the three main SM backgrounds ($ZZ + jets$, $WWZ + jets$, $t\bar{t}Z + jets$). The yellow, cyan, and red filled regions correspond to BP1, BP2, and BP3 respectively, while the blue, green, and magenta colored lines illustrate the $ZZ + jets$, $t\bar{t}Z + jets$ and $WWZ + jets$ background, respectively. Figure 2 suggests that the typical cuts like $p_T^{l_1} > 100$ GeV and a large $m_{\rm eff}$ will reduce the backgrounds significantly without affecting the signal events too much. Following cut optimization, we observe that the $N_l \geq 4 + p_T^{l_1} > 100 + Z$ veto[6] $+ b$ veto cut along with large $m_{\rm eff}$ provides the maximum signal significance. We define the two signal regions as: SR-A with $m_{\rm eff} > 900$ GeV and SR-B with $m_{\rm eff} > 1500$ GeV.

In Table 1, we have summarized the production cross section of the signal benchmark points, the corresponding yields of signal events, and the total background yield after the selection cuts. The signal significance without systematic uncertainty ($\sigma^0_{\rm ss}$) and with 5% uncertainty ($\sigma^5_{\rm ss}$) are also presented in the last three rows. To estimate the signal significance, we have used the relation $\sigma^\epsilon_{\rm ss} = S/\sqrt{S + B + ((S + B)\epsilon)^2}$, where S, B and ϵ correspond to the signal yield, background yield and systematic uncertainty, respectively. Due to the large $m_{\rm eff}$ cut, the SR-B signal regions are more effective than SR-A in the parameter space where slepton masses are relatively higher. The signal significance corresponding to BP1, BP2 and BP3 for the SR-B signal region are 6.77 (6.35), 5.55 (5.31), 1.74 (1.72), respectively, for $\epsilon = 0\%$ (5%). The effect of including 5% uncertainty is not significant and it is observed that the signal significance reduces by 1–6%. We illustrate the projected discovery (5σ) and exclusion (2σ) reach at the HL-LHC using cut-based methods in the $m_{\widetilde{l}_L} - - m_{\widetilde{\chi}^0_1}$ mass plane in Fig. 4. The light-blue filled region denotes the 2σ projection and the blue dotted line corresponds to the projected 5σ discovery reach. The projected exclusion (discovery) curve reaches up to ~ 1.75 (1.49) TeV on slepton masses.

Next, we perform an ML-based analysis for the improvement of signal significance using an extreme gradient boosted decision tree algorithm through XGBoost machine learning toolkit [69]. A set of 18 'features' (kinematic variables) are constructed to perform our analysis which are transverse momenta of leading and subleading lepton ($p_T^{l_1}$ and $p_T^{l_2}$), $\Delta R_{l_i l_j}$ between the first four leading leptons[7] (6 variables), the difference in azimuthal angle $\Delta\phi_{l_i \not{E}_T}$ between first four leading leptons and $\not{E}_T$ (4 variables), number of b-tagged (N_b), non-b-tagged jets (N_j), missing transverse energy ($\not{E}_T$), effective mass ($m_{\rm eff}$), number of SFOS pair ($N_{\rm SFOS}$) and number of reconstructed Z (N_Z). We have considered $N_l \geq 4$ ($l \equiv e, \mu$) events for SUSY signal and SM backgrounds. In this process, 80% of the data set is considered for training and the rest for testing using multi:softprob objective function to achieve the

[5] The effective mass is defined as $m_{\rm eff} = \sum_i p_T^{l_i} + \sum_i p_T^{j_i} + \not{E}_T$.

[6] The event with the same flavor opposite sign leptons pair with invariant mass range $81.2 < m_{\rm SFOS} < 101.2$ GeV are excluded.

[7] ΔR is defined as $\Delta R = \sqrt{(\Delta\eta)^2 + (\Delta\phi)^2}$

multiclass classification. We choose the hyperparameters as follows: `number of trees` = 500, `maximum depth` = 10, and `learning rate` = 0.03 for optimal outcome. Finally, we obtain the predicted probability score of different classes for every event, and applying a threshold on this score we estimate the maximum significance.

To find out the effectiveness of each feature and their ranking we have estimated the Shapley values using SHAP (SHapley Additive exPlanation) [70, 71] toolkit. We plot the mean of absolute values of the top ten kinematic variables in Fig. 3 (left panel) for a particular signal benchmark point, BP2 ($m_{\widetilde{l}_L} = 1450$ GeV, $m_{\widetilde{\chi}_1^0} = 800$ GeV) and SM backgrounds. The top three important variables are N_Z, $\not{E}_T$ and $m_{\rm eff}$. We also depict the effect of probability scores on the signal significance for BP2 with 0 % (blue line) and 5 % (red line) systematic uncertainty in the right panel of Fig. 3. It is evident that the signal significance saturates around probability score $\sim$ 0.9–0.96.

The signal yields, the total background yields, the signal significances for the benchmark points, and the gain in significance from the cut-based analysis are demonstrated in Table 2 for probability score values 0.90 and 0.96. The numbers in the brackets are the results corresponding to significance and gain with 5% systematic uncertainty. Around 15–38% gain in signal significance is achieved by implementing ML algorithms as compared to the cut-based method.

Finally, we estimate the projected discovery (5σ) and exclusion (2σ) reach in the $m_{\widetilde{l}_L} - m_{\widetilde{\chi}_1^0}$ plane at the HL-LHC using ML-based methods. To compare the results with cut-and-count analysis, we present the 5σ and 2σ projection in Fig. 4 using the violet dotted line and violet-colored filled region, respectively. The 5σ and 2σ curves extend up to $\sim$ 1.54 TeV and 1.87 TeV for left-handed degenerate slepton masses (all three generations). This provides us an

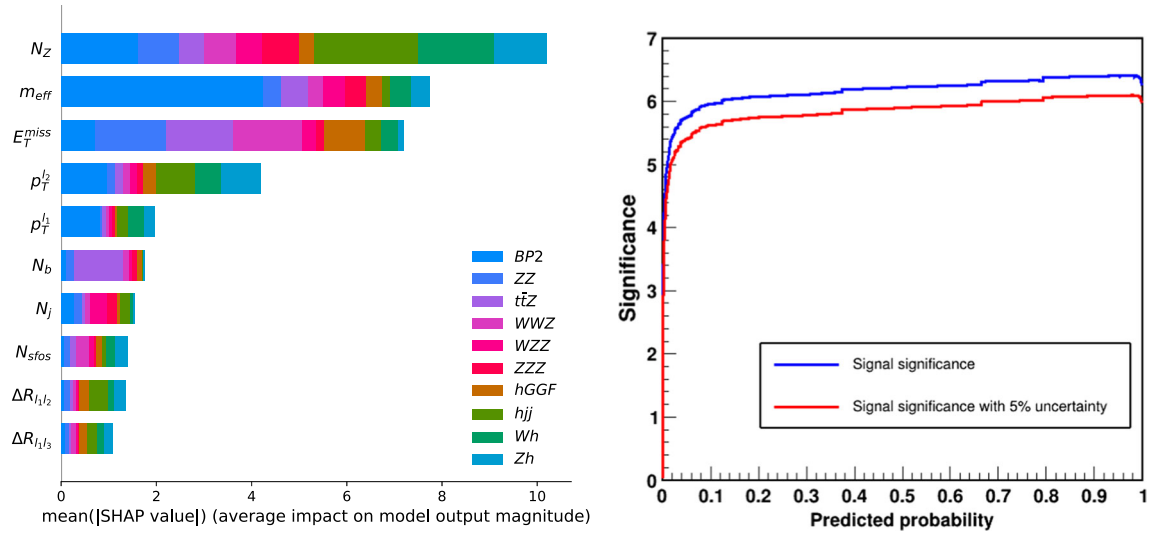

Fig. 3 Left: Shapley feature importance plot for the top ten variables for benchmark point BP2 and the SM backgrounds. Right: the signal significance without any systematic uncertainty and with 5% uncertainty is displayed via blue and red lines as a function of predicted probability

Table 2 Signal yield, total background yield, the signal significance and the gain in significance at the HL-LHC using ML-based algorithm for different probability scores are shown here. In the last two columns, the numbers in the parenthesis correspond to signal significance and gain with systematic uncertainty $\epsilon = 5\%$

Benchmark points	Probability score	Signal yield	Total background yield	Signal significance $\sigma_{\rm ss}$ (sys unc. = 5%)	Gain in $\sigma_{\rm ss}$ from cut-based
BP1	0.90	72.66	3.61	8.32 (7.62)	23% (20%)
	0.96	71.70	1.98	8.35 (7.68)	23% (21%)
BP2	0.90	41.82	1.17	6.38 (6.06)	15% (14%)
	0.96	41.66	0.87	6.39 (6.07)	15% (14%)
BP3	0.90	5.86	0.95	2.25 (2.23)	29% (30%)
	0.96	5.85	0.10	2.40 (2.38)	38% (38%)

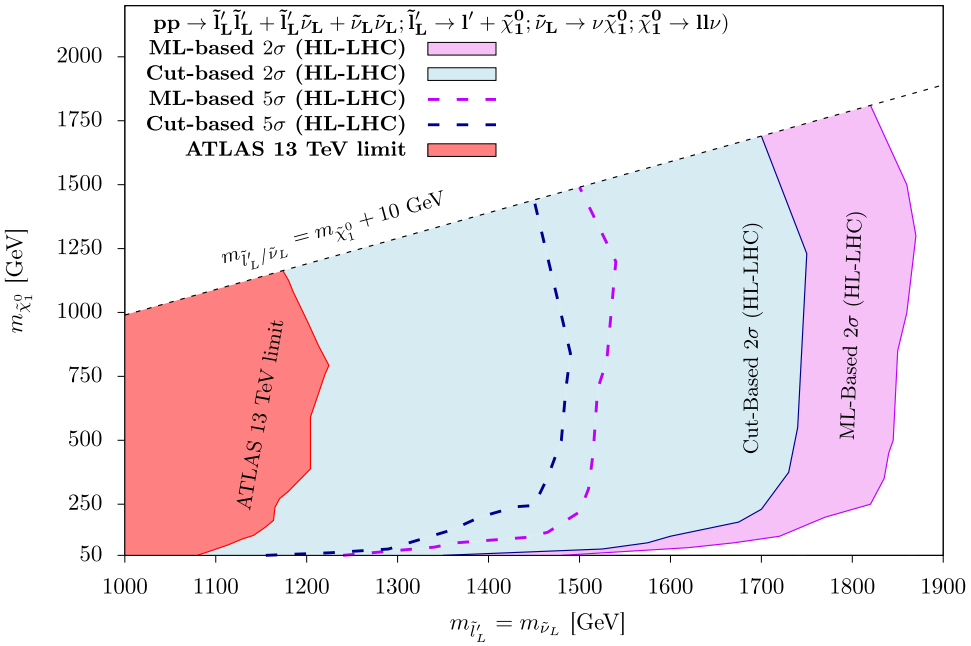

Fig. 4 Projected discovery (5σ) and exclusion (2σ) reach in the slepton–LSP mass plane at the HL-LHC are presented for cut-based and ML-based analysis. The red regions represent the existing limit obtained by the ATLAS collaboration from Run-II data[40]. The violet (blue) regions correspond to 2σ projected reach from the ML-based (cut-and-count) method at the HL-LHC. The blue and violet dotted line stand for 5σ projected discovery reach obtained from traditional cut-based method and `XGBoost`, respectively

enhancement of approximately 120 GeV improvement in the projected exclusion limits using `XGBoost` compared to the cut-based method.

3.2 Prospect at the HE-LHC: cut-based vs. ML analysis

We further extend our analysis for high-energy LHC ($\sqrt{s}$ = 27 TeV, $\mathcal{L}$ = 3000 fb^{-1}) for direct slepton pair production with $N_l \geq 4$ final state. Similar to Sect. 3.1, we implement the cut-and-count method along with an ML-based algorithm for further improvement. To showcase our results and compare the two methods, we have chosen three signal benchmark points as: `BP1` ($m_{\widetilde{l}'_L}$ = 1300 GeV, $m_{\widetilde{\chi}^0_1}$ = 250 GeV), `BP4` ($m_{\widetilde{l}'_L}$ = 2000 GeV, $m_{\widetilde{\chi}^0_1}$ = 1000 GeV) and `BP5` ($m_{\widetilde{l}'_L}$ = 2750 GeV, $m_{\widetilde{\chi}^0_1}$ = 2500 GeV).

Figure 5 depicts the distributions for transverse momenta of leading lepton ($p_T^{l_1}$) and effective mass (m_{eff}) corresponding to these benchmark points and three dominant SM backgrounds channels; ZZ, $t\bar{t}Z$ and WWZ, respectively. We have used similar color conventions for SM backgrounds as in Fig. 2 and `BP1, BP4` and `BP5` are portrayed by yellow, cyan, and red regions, respectively. Similar to the 14 TeV analysis, it is evident that a large cut on $p_T^{l_1}$ and m_{eff} will effectively discard SM backgrounds while merely affecting the signals. We obtain that a cut set consisting of $N_l \geq 4 + Z$ veto + $p_T^{l_1} > 150$ GeV $+b$ veto along with strong m_{eff} cut provides the maximal signal significance. We define two signal regions, `SR-C` with $m_{\text{eff}} > 1500$ GeV and `SR-D` with $m_{\text{eff}} > 2200$ GeV. The cut flow table for selected benchmark points and the total SM backgrounds are presented in Table 3, along with signal significance without and with 5% systematic uncertainty. The signal significance for σ^0_{ss} (σ^5_{ss}) for `BP1`, `BP4` and `BP5` are 22.77 (14.93), 9.04 (8.14), 2.35 (2.31) for `SR-D`.

The projected discovery (5σ) and exclusion (2σ) reach at the HE-LHC using cut-and-count-based method are presented in Fig. 7 in the slepton–LSP mass plane. The light-green shaded region denotes 2σ reach and 5σ reach is denoted by the dotted green line. The current limit obtained from ATLAS collaboration from Run-II data is marked with red color. We have observed that slepton masses can be excluded up to 2.86 (2.82) TeV with the choice of $m_{\widetilde{\chi}^0_1} = 1.9$ (2.81) TeV with 95% C.L. The 5σ projection reaches up to ~ 2.32 TeV for $m_{\widetilde{l}'_L}$ at the HE-LHC with cut-based analysis.

We proceed with a similar ML analysis as in Sect. 3.1 to ascertain how much the sensitivity can be improved upon. We choose the same set of features and hyperparameter selection as discussed earlier. Similar to HL-LHC analysis, we obtain a similar Shapley feature importance plot which is presented in Fig. 6. On the right panel of Fig. 6 we present the variation of signal significance for the HE-LHC as a function of probability score. Next, we

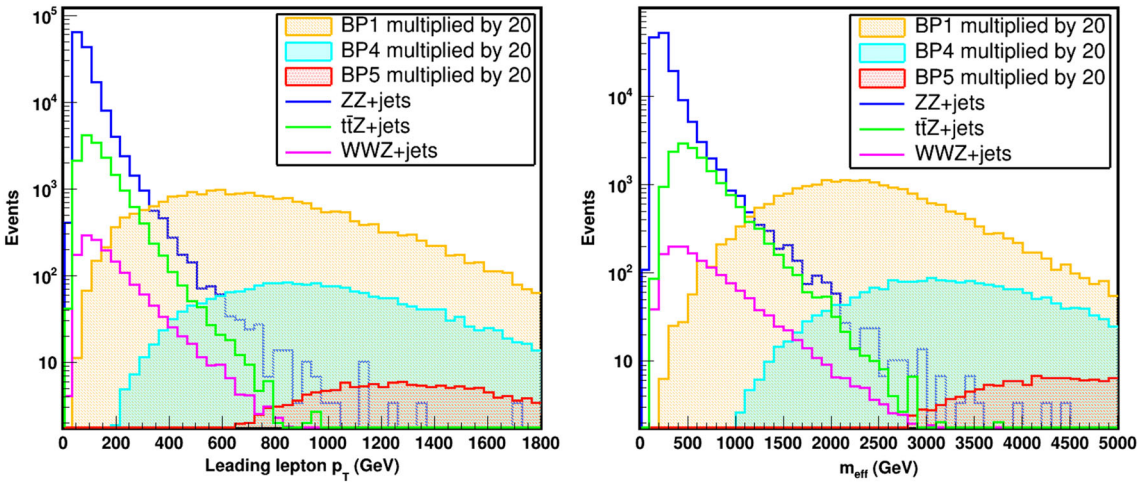

Fig. 5 Distributions of transverse momentum of leading lepton ($p_T^{l_1}$) and effective mass (m_{eff}) at the HE-LHC ($\sqrt{s} = 27$ TeV with $\mathcal{L} = 3000\ fb^{-1}$) are shown here. Color conventions for the SM backgrounds are the same as in Fig. 2. Yellow, cyan, and red filled regions correspond to the benchmark points—`BP1`, `BP4` and `BP5`, respectively (scaled by a factor 20)

Table 3 Cut flow table for signal benchmark points and the total SM backgrounds along with σ_{ss}^0 (σ_{ss}^5) at the HE-LHC are shown here

	$N_l \geq 4$ ($l = e, \mu$) + $p_T^{l_1} > 150$ GeV	Z veto	b veto	Signal region	
				SR-C ($m_{\text{eff}} > 1500$ GeV)	SR-D ($m_{\text{eff}} > 2200$ GeV)
`BP1` (1300,250) $\sigma_{\text{NLO+NLL}}^{27} = 0.628$ fb	1165.63	1032.68	937.85	806.16	524.44
`BP4` (2000,1000) $\sigma_{\text{NLO+NLL}}^{27} = 0.052$ fb	110.79	109.13	98.76	97.40	87.34
`BP5` (2750,2500) $\sigma_{\text{NLO+NLL}}^{27} = 0.0048$ fb	10.24	10.14	9.20	9.19	9.09
Total background	26640.55	708.36	307.57	23.76	5.86
Signal significance σ_{ss}^0 (σ_{ss}^5, sys. unc.=5%)		`BP1`		27.98 (15.96)	22.77 (14.93)
		`BP4`		8.85 (7.75)	9.04 (8.14)
		`BP5`		1.60 (1.54)	2.35 (2.31)

estimate the signal yields, total background yield, and signal significance for different values of probability score and systematic uncertainty for the three benchmark points. We show these results in the Table 4. In the last column, we present the gain in σ_{ss}. An improvement of $\sim 14\%$ to 33% is observed in the `XGBoost` results compared to the conventional cut-based method. The numbers in the parentheses represent the results corresponding to 5% systematic uncertainty. The improvement of signal significance is also echoed in the exclusion plot illustrated in the slepton–LSP mass plane (Fig. 7). The brown dotted line corresponds to the 5σ projections at the HE-LHC using ML-based algorithm and it reaches up to ~ 2.46 TeV. The green dotted line (corresponding to cut-based 5σ) indicates that the reach is enhanced by 140 GeV in the ML-based analysis. We also observe that the projected exclusion curve (displayed via brown solid regions) reaches up to ~ 3.06 TeV resulting in an improvement of $\sim$ 200 GeV as compared to the cut-based method (green region).

3.3 Comparision among different scenarios

In this work, we have focused on the RPV SUSY scenarios with non-zero values of λ_{121} and/or λ_{122} which provide maximum leptonic ($l \equiv e,\ \mu$) branching ratios of the LSP decay and thus leads to the most stringent limits on the slepton masses. Before concluding we comment on the collider limits in other scenarios associated with the remaining seven non-zero λ_{ijk} couplings from $N_l \geq 4$ ($l \equiv e, \mu$) final state. The scenarios with non-zero λ_{121} and/or λ_{122}, for which we already obtained the limits in Sects. 3.1 and 3.2 are denoted as **S-I**.

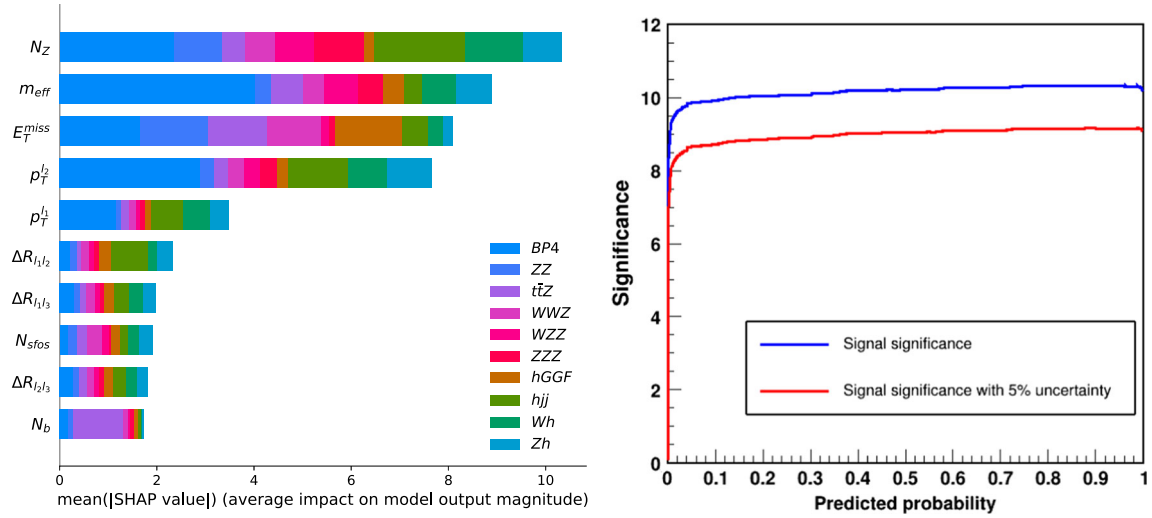

Fig. 6 Left: Shapley feature importance plot for the top ten variables for benchmark point BP4 and the SM backgrounds. Right: the signal significance at the HE-LHC without any systematic uncertainty and with 5% uncertainty are displayed via blue and red lines as a function of predicted probability

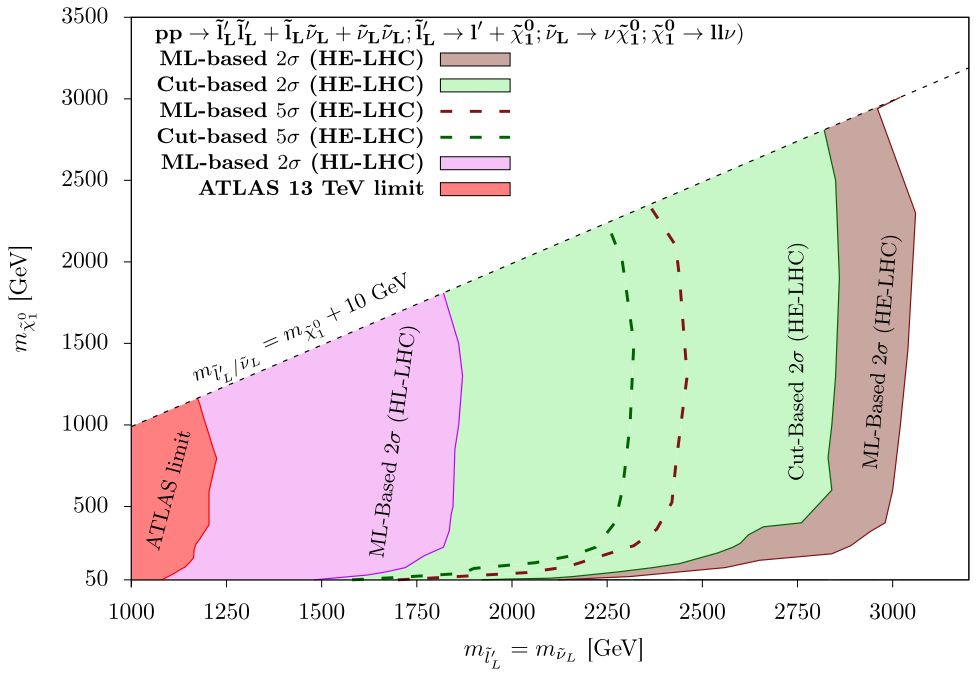

Fig. 7 Projected discovery (5σ) and exclusion (2σ) reach in the slepton–LSP mass plane at the HE-LHC are presented for cut-based and ML-based analysis. The red regions represent the existing limit obtained by the ATLAS collaboration from Run-II data [40]. The violet regions correspond to 2σ projected reach from the ML-based method at the HL-LHC as shown in Fig. 4. The 5σ projected discovery reach obtained from traditional cut-based method and `XGBoost` are shown via green and brown dotted lines, respectively. The green and brown solid regions stand for 2σ projected to reach from cut-based and ML-based methods respectively at the HE-LHC

- *Scenario-II* **S-II** represents the models with single non zero couplings λ_{i3k} where $i \equiv 1,\ 2$ and $k \equiv 1,\ 2$. The LSP pair in the final state decays to $4l$, $3l1\tau$, and $2l2\tau$ final states with 25%, 50%, and 25% branching ratios, respectively.
- *Scenario-III* **S-III** defines the model with non-zero value of λ_{123} coupling where we get $2l2\tau$ final state with 100% branching ratio from the LSP pair.
- *Scenario-IV* **S-IV** corresponds to the non-zero values of λ_{i33} with $i \equiv 1,\ 2$ where the LSP pair decays to $2l2\tau$, $1l3\tau$ and 4τ final states with 25%, 50% and 25% branching ratios, respectively.

Table 4 Signal yield, total background yield, the signal significance and the gain in significance at the HE-LHC using ML-based algorithm for different probability scores are shown here. In the last two columns, the numbers in the parenthesis correspond to signal significance and gain with systematic uncertainty $\epsilon = 5\%$

Benchmark points	Probability score	Signal	Total background yield	Signal significance σ_{ss} (sys unc. = 5%)	Gain in σ_{ss} from cut-based
BP1	0.90	1098.85	10.73	32.98 (16.98)	18% (6%)
	0.96	1080.31	4.18	32.80 (17.02)	17% (6%)
BP4	0.90	107.68	1.23	10.31 (9.14)	14% (12%)
	0.96	107.40	0.48	10.34 (9.18)	14% (12%)
BP5	0.90	9.92	0.21	3.11 (3.07)	32% (33%)
	0.96	9.90	0.18	3.12 (3.08)	33% (33%)

Table 5 Comparison of signal significance of signal benchmark points at the HL-LHC and HE-LHC for different model scenarios using ML-based analysis

HL-LHC					HE-LHC				
Benchmark points	Signal significance				Benchmark	Signal significance			
	S-I	S-II	S-III	S-IV	points	S-I	S-II	S-III	S-IV
BP1	8.35	6.69	4.84	3.52	BP1	32.98	26.64	18.86	13.50
BP2	6.39	5.25	3.86	2.83	BP4	10.31	8.46	6.26	4.59
BP3	2.40	1.91	1.32	0.93	BP5	3.11	2.51	1.76	1.18
$m_{\tilde{\chi}_1^0}$ [GeV]	Exclusion limit on $m_{\tilde{l}'} = m_{\tilde{\nu}_L}$ [GeV]				$m_{\tilde{\chi}_1^0}$ [GeV]	Exclusion limit on $m_{\tilde{l}'} = m_{\tilde{\nu}_L}$ [GeV]			
800	1850	1800	1670	1575	1000	3020	2880	2620	2500

- The nine independent non-zero LLE RPV couplings lead to these four scenarios which have been tabulated in Appendix A.
- Among these four scenarios, the $N_l \geq 4$ ($l = e, \mu$) channel provides the best limit in **S-I** models. On the other hand, one expects the weakest limit in **S-IV** model which is mostly tau enriched. Discovery and exclusion reach in other two models (**S-III** and **S-IV**) or models with any arbitrary combination of non-zero λ_{ijk} lie between **S-I** and **S-IV**. This pattern is observed in Table 5 where we present the signal significance obtained from ML-based analysis at the HL-LHC and HE-LHC for the above-mentioned four models.
- In Table 5, we also show the variation of projected 2σ limits on slepton mass for a fixed choice of LSP mass. We observe that the limits are weaker by 275 (520) GeV at the HL-LHC and HE-LHC in the extreme tau enriched model, i.e., **S-IV** compared to **S-I**.

4 Conclusion

Supersymmetric signals have been searched extensively at the LHC. The R-parity conserving framework has typically been more widely studied compared to its R-parity violating counterpart. The large number of final states non-zero R-parity violating couplings can open up a need to be studied to ascertain the full extent of impact the LHC data has or is going to have on the relevant parameter space. Sleptons are of particular importance in the context of any SUSY scenarios since they affect the contribution of the model to some very crucial observables, such as light neutrino mass and mixing, lepton magnetic moment, and lepton number or lepton flavor violating decay rates. Non-zero λ couplings also contribute to these observables. In this work, therefore, we have explored a scenario where the sleptons and sneutrinos are produced through usual RPC couplings and subsequently decay into leptons and neutrinos through RPV decay of the bino LSP. To understand the maximum impact LHC can have on the parameter space, we consider the production of all three generations of sneutrinos and left-handed sleptons which have larger cross sections compared to their right-handed counterpart. We have performed a detailed cut-based collider analysis alongside using a machine learning algorithm for comparison. Since we are interested in electron

and muon-enriched final states, we have only considered non-zero λ_{121} and λ_{122} couplings. Our final state has rich lepton multiplicity, $N_l \geq 4$ ($l \equiv e, \mu$). We observe that this final state can probe slepton and sneutrino masses most efficiently. In our analysis, we have assumed the left-handed sleptons and sneutrinos to be mass degenerate for simplicity. We explore both the high-luminosity and high-energy options of the LHC and present our results in terms of exclusion region (2σ statistical significance) and discovery reach (5σ statistical significance) in the LSP–slepton/sneutrino mass plane. Our study reveals that the discovery regions reach up to $\sim$ 1.49 TeV and $\sim$ 1.54 TeV, while the exclusion regions reach up to $\sim$ 1.75 TeV and $\sim$ 1.87 TeV at HL-LHC for cut-based and ML algorithm, respectively. Similarly at HE-LHC, we have shown that the projected discovery regions reach up to $\sim$ 2.32 TeV and $\sim$ 2.46 TeV, while the projected exclusion limits are $\sim$ 2.86 TeV and $\sim$ 3.06 TeV for cut-based and ML algorithm, respectively. We obtain overall better improvement in the case of HE-LHC with ML algorithm. Understandably, the presence of other non-zero λ couplings can give rise to τ-leptons in the final states and as a result reduces the signal efficiency. We have compared the different possible scenarios with different non-zero λ couplings. We observed that in the worst case scenario when only the λ_{i33} ($i = 1, 2$) are non-zero, the signal significance drops by a factor of $\sim$ 2.2−2.6 at HL-LHC and HE-LHC.

Data availability No data associated in the manuscript.

The branching ratios of LSP decay depending upon λ_{ijk} coupling and their contribution to the final state

See Tables 6 and 7.

Table 6 All possible LSP decay modes for different RPV coupling (λ_{ijk}) choices corresponding to different i, j and k values. Final state e and ν_e are marked using blue, μ and ν_μ are marked using magenta, and τ and ν_τ are marked using cyan color, respectively

	$ij = 12$	$ij = 13$	$ij = 23$
$k = 1$	$ee\nu_\mu$ (50%), $e\mu\nu_e$ (50%)	$ee\nu_\tau$ (50%), $e\tau\nu_e$ (50%)	$e\mu\nu_\tau$ (50%), $e\tau\nu_\mu$ (50%)
$k = 2$	$\mu e\nu_\mu$ (50%), $\mu\mu\nu_e$ (50%)	$\mu e\nu_\tau$ (50%), $\mu\tau\nu_e$ (50%)	$\mu\mu\nu_\tau$ (50%), $\mu\tau\nu_\mu$ (50%)
$k = 3$	$\tau e\nu_\mu$ (50%), $\tau\mu\nu_e$ (50%)	$\tau e\nu_\tau$ (50%), $\tau\tau\nu_e$ (50%)	$\tau\mu\nu_\tau$ (50%), $\tau\tau\nu_\mu$ (50%)

Table 7 Final state configuration coming from the LSP pair through different non-vanishing RPV LLE couplings. Depending upon the final state leptonic branching ratios, four scenarios are defined (S-I to S-IV). Final state electron, muon and tau are marked using blue, magenta and cyan color, respectively

Scenarios	Non-vanishing λ_{ijk} couplings	Final State configuration (Branching Ratio)			Final state ($l = e, \mu$)
S-I	λ_{121}	$4e$(25%)	$3e1\mu$(50%)	$2e2\mu$(25%)	$4l$ (100%)
	λ_{122}	4μ(25%)	$3\mu1e$(50%)	$2e2\mu$(25%)	
S-II	λ_{131}	$4e$(25%)	$3e1\tau$(50%)	$2e2\tau$(25%)	$4l$(25%)
	λ_{232}	4μ(25%)	$3\mu1\tau$(50%)	$2\mu2\tau$(25%)	$3l1\tau$(50%)
	λ_{132}	$2\mu2e$(25%)	$1e2\mu1\tau$(50%)	$2\mu2\tau$(25%)	$2l2\tau$(25%)
	λ_{231}	$2e2\mu$(25%)	$2e1\mu1\tau$(50%)	$2e2\tau$(25%)	
S-III	λ_{123}	$2e2\tau$(25%)	$1e1\mu2\tau$(50%)	$2\mu2\tau$(25%)	$2l2\tau$(100%)
S-IV	λ_{133}	$2e2\tau$(25%)	$1e3\tau$(50%)	4τ(25%)	$2l2\tau$(25%)
	λ_{233}	$2\mu2\tau$(25%)	$1\mu3\tau$(50%)	4τ(25%)	$1l3\tau$(50%)
					4τ(25%)

Individual contributions of different production channels for the benchmark points

See Table 8.

Table 8 Cross sections of three production channels for benchmark points in the HL-LHC and HE-LHC analysis. The masses are in GeV

HL-LHC			HE-LHC		
Benchmark Points	Production Channel	Cross section (NLO+NLL) in fb	Benchmark Points	Production Channel	Cross section (NLO+NLL) in fb
BP1	$pp \to \tilde{l}'_L \tilde{l}'_L$	7.04×10^{-3}	BP1	$pp \to \tilde{l}'_L \tilde{l}'_L$	1.038×10^{-1}
$m_{\tilde{l}'_{L/\tilde{\nu}}} = 1300$	$pp \to \tilde{l}'_L \tilde{\nu}$	2.529×10^{-2}	$m_{\tilde{l}'_{L/\tilde{\nu}}} = 1300$	$pp \to \tilde{l}'_L \tilde{\nu}$	4.308×10^{-1}
$m_{\tilde{\chi}^0_1} = 250$	$pp \to \tilde{\nu}\tilde{\nu}$	5.79×10^{-3}	$m_{\tilde{\chi}^0_1} = 250$	$pp \to \tilde{\nu}\tilde{\nu}$	9.33×10^{-2}
	σ^{Total}	$\mathbf{3.81 \times 10^{-2}}$		σ^{Total}	$\mathbf{6.28 \times 10^{-1}}$
BP2	$pp \to \tilde{l}'_L \tilde{l}'_L$	3.58×10^{-3}	BP4	$pp \to \tilde{l}'_L \tilde{l}'_L$	8.89×10^{-3}
$m_{\tilde{l}'_{L/\tilde{\nu}}} = 1450$	$pp \to \tilde{l}'_L \tilde{\nu}$	1.304×10^{-2}	$m_{\tilde{l}'_{L/\tilde{\nu}}} = 2000$	$pp \to \tilde{l}'_L \tilde{\nu}$	3.553×10^{-2}
$m_{\tilde{\chi}^0_1} = 800$	$pp \to \tilde{\nu}\tilde{\nu}$	2.97×10^{-3}	$m_{\tilde{\chi}^0_1} = 1000$	$pp \to \tilde{\nu}\tilde{\nu}$	7.71×10^{-3}
	σ^{Total}	$\mathbf{1.96 \times 10^{-2}}$		σ^{Total}	$\mathbf{5.2 \times 10^{-2}}$
BP3	$pp \to \tilde{l}'_L \tilde{l}'_L$	5.95×10^{-4}	BP5	$pp \to \tilde{l}'_L \tilde{l}'_L$	8.56×10^{-4}
$m_{\tilde{l}'_{L/\tilde{\nu}}} = 1800$	$pp \to \tilde{l}'_L \tilde{\nu}$	1.829×10^{-3}	$m_{\tilde{l}'_{L/\tilde{\nu}}} = 2750$	$pp \to \tilde{l}'_L \tilde{\nu}$	3.19×10^{-3}
$m_{\tilde{\chi}^0_1} = 1750$	$pp \to \tilde{\nu}\tilde{\nu}$	4.73×10^{-4}	$m_{\tilde{\chi}^0_1} = 2500$	$pp \to \tilde{\nu}\tilde{\nu}$	7.1×10^{-4}
	σ^{Total}	$\mathbf{2.9 \times 10^{-3}}$		σ^{Total}	$\mathbf{4.8 \times 10^{-3}}$

References

1. Drees, M., Godbole, R., Roy, P.: Theory and phenomenology of Sparticles: an account of four-dimensional $N = 1$ supersymmetry in high energy physics. (2004)
2. Haber, H.E., Stephenson Haskins, L.: Supersymmetric theory and models. In: Theoretical Advanced Study Institute in Elementary Particle Physics: Anticipating the Next Discoveries in Particle Physics, pp. 355–499 (2018). https://doi.org/10.1142/9789813233348_0006
3. S.P. Martin, A supersymmetry primer. Adv. Ser. Direct. High Energy Phys. **18**, 1–98 (1998). https://doi.org/10.1142/9789812839657_0001
4. H.P. Nilles, Supersymmetry, supergravity and particle physics. Phys. Rep. **110**, 1–162 (1984). https://doi.org/10.1016/0370-1573(84)90008-5
5. L. Susskind, The gauge hierarchy problem, technicolor, supersymmetry, and all that. Phys. Rep. **104**(2), 181–193 (1984). https://doi.org/10.1016/0370-1573(84)90208-4
6. E. Gildener, Gauge-symmetry hierarchies. Phys. Rev. D **14**, 1667–1672 (1976). https://doi.org/10.1103/PhysRevD.14.1667
7. Aghanim, N., et al.: Planck 2018 results. VI. Cosmological parameters. Astron. Astrophys. **641**, 6 (2020). https://doi.org/10.1051/0004-6361/201833910. arXiv:1807.06209 [astro-ph.CO]. [Erratum: Astron. Astrophys. 652, C4 (2021)]
8. B. Abi et al., Measurement of the positive muon anomalous magnetic moment to 0.46 ppm. Phys. Rev. Lett. **126**(14), 141801 (2021). https://doi.org/10.1103/PhysRevLett.126.141801. arXiv:2104.03281 [hep-ex]
9. CMS SUSY public result. https://cms-results.web.cern.ch/cms-results/public-results/preliminary-results/SUS/index.html
10. Atlas SUSY public result. https://twiki.cern.ch/twiki/bin/view/AtlasPublic/SupersymmetryPublicResults
11. Vempati, S.K.: Introduction to MSSM (2012). arXiv:1201.0334 [hep-ph]
12. G. Bertone, D. Hooper, J. Silk, Particle dark matter: evidence, candidates and constraints. Phys. Rep. **405**, 279–390 (2005). https://doi.org/10.1016/j.physrep.2004.08.031. arXiv:hep-ph/0404175
13. Baer, H., Tata, X.: In: Datta, A., Mukhopadhyaya, B., Raychaudhuri, A., Gupta, A.K., Khetrapal, C.L., Padmanabhan, T., Vijayan, M. (eds.) Dark matter and the LHC, pp. 179–203 (2009). https://doi.org/10.1007/978-81-8489-295-6_12

14. L. Roszkowski, Particle dark matter: a theorist's perspective. Pramana **62**, 389–401 (2004). https://doi.org/10.1007/BF02705097. arXiv:hep-ph/0404052
15. G. Jungman, M. Kamionkowski, K. Griest, Supersymmetric dark matter. Phys. Rep. **267**, 195–373 (1996). https://doi.org/10.1016/0370-1573(95)00058-5. arXiv:hep-ph/9506380
16. R.K. Barman, G. Bélanger, B. Bhattacherjee, R.M. Godbole, R. Sengupta, Is light neutralino thermal dark matter in the phenomenological minimal supersymmetric standard model ruled out? Phys. Rev. Lett. **131**(1), 011802 (2023). https://doi.org/10.1103/PhysRevLett.131.011802. arXiv:2207.06238 [hep-ph]
17. He, Y., Jia, X., Meng, L., Yue, Y., Zhang, D.: Impact of recent measurement of $(g-2)_\mu$, LHC search for supersymmetry, and LZ experiment on minimal supersymmetric standard model. (2023). arXiv:2303.02360 [hep-ph]
18. M. Chakraborti, U. Chattopadhyay, S. Poddar, How light a Higgsino or a wino dark matter can become in a compressed scenario of MSSM. JHEP **09**, 064 (2017). https://doi.org/10.1007/JHEP09(2017)064. arXiv:1702.03954 [hep-ph]
19. D. Chowdhury, K.M. Patel, X. Tata, S.K. Vempati, Indirect searches of the degenerate MSSM. Phys. Rev. D **95**(7), 075025 (2017). https://doi.org/10.1103/PhysRevD.95.075025. arXiv:1612.06471 [hep-ph]
20. N. Bhattacharyya, A. Choudhury, A. Datta, Low mass neutralino dark matter in mSUGRA and more general models in the light of LHC data. Phys. Rev. D **84**, 095006 (2011). https://doi.org/10.1103/PhysRevD.84.095006. arXiv:1107.1997 [hep-ph]
21. A. Choudhury, A. Datta, Many faces of low mass neutralino dark matter in the unconstrained MSSM, LHC data and new signals. JHEP **06**, 006 (2012). https://doi.org/10.1007/JHEP06(2012)006. arXiv:1203.4106 [hep-ph]
22. A. Choudhury, A. Datta, Neutralino dark matter confronted by the LHC constraints on electroweak SUSY signals. JHEP **09**, 119 (2013). https://doi.org/10.1007/JHEP09(2013)119. arXiv:1305.0928 [hep-ph]
23. M. Chakraborti, L. Roszkowski, S. Trojanowski, GUT-constrained supersymmetry and dark matter in light of the new $(g-2)_\mu$ determination. JHEP **05**, 252 (2021). https://doi.org/10.1007/JHEP05(2021)252. arXiv:2104.04458 [hep-ph]
24. A. Choudhury, S. Mondal, Revisiting the exclusion limits from direct chargino–neutralino production at the LHC. Phys. Rev. D **94**(5), 055024 (2016). https://doi.org/10.1103/PhysRevD.94.055024. arXiv:1603.05502 [hep-ph]
25. J. Dutta, P. Konar, S. Mondal, B. Mukhopadhyaya, S.K. Rai, A revisit to a compressed supersymmetric spectrum with 125 GeV Higgs. JHEP **01**, 051 (2016). https://doi.org/10.1007/JHEP01(2016)051. arXiv:1511.09284 [hep-ph]
26. J. Dutta, P. Konar, S. Mondal, B. Mukhopadhyaya, S.K. Rai, Search for a compressed supersymmetric spectrum with a light gravitino. JHEP **09**, 026 (2017). https://doi.org/10.1007/JHEP09(2017)026. arXiv:1704.04617 [hep-ph]
27. H.K. Dreiner, an introduction to explicit R-parity violation. Adv. Ser. Direct. High Energy Phys. **21**, 565–583 (2010). https://doi.org/10.1142/9789814307505_0017. arXiv:hep-ph/9707435
28. R. Barbier et al., R-parity violating supersymmetry. Phys. Rep. **420**, 1–202 (2005). https://doi.org/10.1016/j.physrep.2005.08.006. arXiv:hep-ph/0406039
29. T. Banks, Y. Grossman, E. Nardi, Y. Nir, Supersymmetry without R-parity and without lepton number. Phys. Rev. D **52**, 5319–5325 (1995). https://doi.org/10.1103/PhysRevD.52.5319. arXiv:hep-ph/9505248
30. A. Choudhury, A. Mondal, S. Mondal, Status of R-parity violating SUSY. arXiv:2402.04040 [hep-ph]
31. Y. Grossman, S. Rakshit, Neutrino masses in R-parity violating supersymmetric models. Phys. Rev. D **69**, 093002 (2004). https://doi.org/10.1103/PhysRevD.69.093002. arXiv:hep-ph/0311310
32. J.E. Kim, B. Kyae, H.M. Lee, Effective supersymmetric theory and (g-2)(muon with R-parity violation. Phys. Lett. B **520**, 298–306 (2001). https://doi.org/10.1016/S0370-2693(01)01134-0. arXiv:hep-ph/0103054
33. A. Chakraborty, S. Chakraborty, Probing $(g-2)_\mu$ at the LHC in the paradigm of R-parity violating MSSM. Phys. Rev. D **93**(7), 075035 (2016). https://doi.org/10.1103/PhysRevD.93.075035. arXiv:1511.08874 [hep-ph]
34. H.K. Dreiner, Y.S. Koay, D. Köhler, V.M. Lozano, J. Montejo Berlingen, S. Nangia, N. Strobbe, The ABC of RPV: classification of R-parity violating signatures at the LHC for small couplings. JHEP **07**, 215 (2023). https://doi.org/10.1007/JHEP07(2023)215. arXiv:2306.07317 [hep-ph]
35. V.A. Mitsou, R-parity violating supersymmetry and neutrino physics: experimental signatures. PoS **PLANCK2015**, 085 (2015). https://doi.org/10.22323/1.258.0085. arXiv:1510.02660 [hep-ph]
36. D. Bardhan, A. Chakraborty, D. Choudhury, D.K. Ghosh, M. Maity, Search for bottom squarks in the baryon-number violating MSSM. Phys. Rev. D **96**(3), 035024 (2017). https://doi.org/10.1103/PhysRevD.96.035024. arXiv:1611.03846 [hep-ph]
37. B. Bhattacherjee, A. Chakraborty, Study of the baryonic R-parity violating MSSM using the jet substructure technique at the 14 TeV LHC. Phys. Rev. D **89**(11), 115016 (2014). https://doi.org/10.1103/PhysRevD.89.115016. arXiv:1311.5785 [hep-ph]
38. B. Bhattacherjee, J.L. Evans, M. Ibe, S. Matsumoto, T.T. Yanagida, Natural supersymmetry's last hope: R-parity violation via UDD operators. Phys. Rev. D **87**(11), 115002 (2013). https://doi.org/10.1103/PhysRevD.87.115002. arXiv:1301.2336 [hep-ph]
39. D. Dercks, J. De Vries, H.K. Dreiner, Z.S. Wang, R-parity violation and light neutralinos at CODEX-b, FASER, and MATHUSLA. Phys. Rev. D **99**(5), 055039 (2019). https://doi.org/10.1103/PhysRevD.99.055039. arXiv:1810.03617 [hep-ph]
40. G. Aad et al., Search for supersymmetry in events with four or more charged leptons in 139 fb^{-1} of $\sqrt{s} = 13$ TeV pp collisions with the ATLAS detector. JHEP **07**, 167 (2021). https://doi.org/10.1007/JHEP07(2021)167. arXiv:2103.11684 [hep-ex]
41. G.W. Bennett et al., Final report of the muon E821 anomalous magnetic moment measurement at BNL. Phys. Rev. D **73**, 072003 (2006). https://doi.org/10.1103/PhysRevD.73.072003. arXiv:hep-ex/0602035

42. Aguillard, D.P., et al.: Measurement of the positive muon anomalous magnetic moment to 0.20 ppm. (2023). arXiv:2308.06230 [hep-ex]
43. M. Chakraborti, S. Iwamoto, J.S. Kim, R. Masełek, K. Sakurai, Supersymmetric explanation of the muon g-2 anomaly with and without stable neutralino. JHEP **08**, 124 (2022). https://doi.org/10.1007/JHEP08(2022)124. arXiv:2202.12928 [hep-ph]
44. Choudhury, A., Mitra, S., Mondal, A., Mondal, S.: Bilinear R-parity violating supersymmetry under the light of neutrino oscillation, Higgs and flavor data. (2023). arXiv:2305.15211 [hep-ph]
45. M. Chakraborti, U. Chattopadhyay, A. Choudhury, A. Datta, S. Poddar, Reduced LHC constraints for Higgsino-like heavier electroweakinos. JHEP **11**, 050 (2015). https://doi.org/10.1007/JHEP11(2015)050. arXiv:1507.01395 [hep-ph]
46. M. Chakraborti, U. Chattopadhyay, A. Choudhury, A. Datta, S. Poddar, The electroweak sector of the pMSSM in the light of LHC-8 TeV and other data. JHEP **07**, 019 (2014). https://doi.org/10.1007/JHEP07(2014)019. arXiv:1404.4841 [hep-ph]
47. H. Baer, V. Barger, H. Serce, Anomalous muon magnetic moment, supersymmetry, naturalness, LHC search limits and the landscape. Phys. Lett. B **820**, 136480 (2021). https://doi.org/10.1016/j.physletb.2021.136480. arXiv:2104.07597 [hep-ph]
48. M. Endo, K. Hamaguchi, S. Iwamoto, T. Kitahara, Supersymmetric interpretation of the muon g-2 anomaly. JHEP **07**, 075 (2021). https://doi.org/10.1007/JHEP07(2021)075. arXiv:2104.03217 [hep-ph]
49. A. Choudhury, S. Rao, L. Roszkowski, Impact of LHC data on muon $g-2$ solutions in a vectorlike extension of the constrained MSSM. Phys. Rev. D **96**(7), 075046 (2017). https://doi.org/10.1103/PhysRevD.96.075046. arXiv:1708.05675 [hep-ph]
50. K. Kowalska, L. Roszkowski, E.M. Sessolo, A.J. Williams, GUT-inspired SUSY and the muon g − 2 anomaly: prospects for LHC 14 TeV. JHEP **06**, 020 (2015). https://doi.org/10.1007/JHEP06(2015)020. arXiv:1503.08219 [hep-ph]
51. R.S. Hundi, Constraints from neutrino masses and muon (g-2) in the bilinear R-parity violating supersymmetric model. Phys. Rev. D **83**, 115019 (2011). https://doi.org/10.1103/PhysRevD.83.115019. arXiv:1101.2810 [hep-ph]
52. W. Altmannshofer, P.S.B. Dev, A. Soni, Y. Sui, Addressing $R_{D^{(*)}}$, $R_{K^{(*)}}$, muon $g-2$ and ANITA anomalies in a minimal R-parity violating supersymmetric framework. Phys. Rev. D **102**(1), 015031 (2020). https://doi.org/10.1103/PhysRevD.102.015031. arXiv:2002.12910 [hep-ph]
53. M.-D. Zheng, H.-H. Zhang, Studying the $b \to s\ell^+\ell^-$ anomalies and $(g-2)_\mu$ in R-parity violating MSSM framework with the inverse seesaw mechanism. Phys. Rev. D **104**(11), 115023 (2021). https://doi.org/10.1103/PhysRevD.104.115023. arXiv:2105.06954 [hep-ph]
54. M.-D. Zheng, F.-Z. Chen, H.-H. Zhang, Explaining anomalies of B-physics, muon $g-2$ and W mass in R-parity violating MSSM with seesaw mechanism. Eur. Phys. J. C **82**(10), 895 (2022). https://doi.org/10.1140/epjc/s10052-022-10822-y. arXiv:2207.07636 [hep-ph]
55. A. Choudhury, A. Mondal, S. Mondal, S. Sarkar, Improving sensitivity of trilinear R-parity violating SUSY searches using machine learning at the LHC. Phys. Rev. D **109**(3), 035001 (2024). https://doi.org/10.1103/PhysRevD.109.035001. arXiv:2308.02697 [hep-ph]
56. R.K. Barman, B. Bhattacherjee, I. Chakraborty, A. Choudhury, N. Khan, Electroweakino searches at the HL-LHC in the baryon number violating MSSM. Phys. Rev. D **103**(1), 015003 (2021). https://doi.org/10.1103/PhysRevD.103.015003. arXiv:2003.10920 [hep-ph]
57. A.S. Cornell, W. Doorsamy, B. Fuks, G. Harmsen, L. Mason, Boosted decision trees in the era of new physics: a smuon analysis case study. JHEP **04**, 015 (2022). https://doi.org/10.1007/JHEP04(2022)015. arXiv:2109.11815 [hep-ph]
58. Coadou, Y.: Boosted decision trees (2022). https://doi.org/10.1142/9789811234033_0002. arXiv:2206.09645 [physics.data-an]
59. B. Fuks, M. Klasen, D.R. Lamprea, M. Rothering, Revisiting slepton pair production at the large hadron collider. JHEP **01**, 168 (2014). https://doi.org/10.1007/JHEP01(2014)168. arXiv:1310.2621 [hep-ph]
60. J. Fiaschi, M. Klasen, Slepton pair production at the LHC in NLO+NLL with resummation-improved parton densities. JHEP **03**, 094 (2018). https://doi.org/10.1007/JHEP03(2018)094. arXiv:1801.10357 [hep-ph]
61. J. Fiaschi, B. Fuks, M. Klasen, A. Neuwirth, Electroweak superpartner production at 13.6 Tev with resummino. Eur. Phys. J. C **83**(8), 707 (2023). https://doi.org/10.1140/epjc/s10052-023-11888-y. arXiv:2304.11915 [hep-ph]
62. G. Bozzi, B. Fuks, M. Klasen, Threshold resummation for slepton-pair production at hadron colliders. Nucl. Phys. B **777**, 157–181 (2007). https://doi.org/10.1016/j.nuclphysb.2007.03.052. arXiv:hep-ph/0701202
63. B. Fuks, M. Klasen, D.R. Lamprea, M. Rothering, Precision predictions for electroweak superpartner production at hadron colliders with resummino. Eur. Phys. J. C **73**, 2480 (2013). https://doi.org/10.1140/epjc/s10052-013-2480-0. arXiv:1304.0790 [hep-ph]
64. Beenakker, W., Klasen, M., Kramer, M., Plehn, T., Spira, M., Zerwas, P.M.: The Production of charginos/neutralinos and sleptons at hadron colliders. Phys. Rev. Lett. 83, 3780–3783 (1999). https://doi.org/10.1103/PhysRevLett.100.029901. arXiv:hep-ph/9906298. [Erratum: Phys. Rev. Lett. 100, 029901 (2008)]
65. J. Alwall, R. Frederix, S. Frixione, V. Hirschi, F. Maltoni, O. Mattelaer, H.-S. Shao, T. Stelzer, P. Torrielli, M. Zaro, The automated computation of tree-level and next-to-leading order differential cross sections, and their matching to parton shower simulations. JHEP **07**, 079 (2014). https://doi.org/10.1007/JHEP07(2014)079. arXiv:1405.0301 [hep-ph]
66. T. Sjostrand, S. Mrenna, P.Z. Skands, PYTHIA 6.4 physics and manual. JHEP **05**, 026 (2006). https://doi.org/10.1088/1126-6708/2006/05/026. arXiv:hep-ph/0603175

67. J. Favereau, C. Delaere, P. Demin, A. Giammanco, V. Lemaître, A. Mertens, M. Selvaggi, DELPHES 3, A modular framework for fast simulation of a generic collider experiment. JHEP **02**, 057 (2014). https://doi.org/10.1007/JHEP02(2014)057. arXiv:1307.6346 [hep-ex]
68. M. Cacciari, G.P. Salam, G. Soyez, The anti-k_t jet clustering algorithm. JHEP **04**, 063 (2008). https://doi.org/10.1088/1126-6708/2008/04/063. arXiv:0802.1189 [hep-ph]
69. Chen, T., Guestrin, C.: XGBoost: a scalable tree boosting system. (2016). https://doi.org/10.1145/2939672.2939785. arXiv:1603.02754 [cs.LG]
70. Lundberg, S.M., Lee, S.: A unified approach to interpreting model predictions. CoRR arXiv:1705.07874 (2017)
71. L.S. Shapley, Xxx, in *17. A Value for n-Person Games*. ed. by H.W. Kuhn, A.W. Tucker (Princeton, Princeton University Press, 1953), pp.307–318. https://doi.org/10.1515/9781400881970-018